Fluorescence Spectrum and Thermalization in a Driven Coupled Cavity Array

Dainius Kilda and Jonathan Keeling
SUPA, School of Physics and Astronomy, University of St. Andrews, St. Andrews KY16 9SS, United Kingdom

(Received 23 September 2017; revised manuscript received 4 December 2018; published 1 February 2019)

We calculate the fluorescence spectra of a driven lattice of coupled cavities. To do this, we extend methods of evaluating two-time correlations in infinite lattices to open quantum systems; this allows access to momentum-resolved fluorescence spectrum. We illustrate this for a driven-dissipative transverse-field anisotropic XY model. By studying the fluctuation-dissipation theorem, we find the emergence of a quasithermalized steady state with a temperature dependent on system parameters; for blue-detuned driving, we show this effective temperature is negative. In the low excitation density limit, we compare these numerical results to analytical spin-wave theory, providing an understanding of the form of the distribution function and the origin of quasithermalization.

DOI: 10.1103/PhysRevLett.122.043602

By driving a system out of equilibrium, it is possible to stabilize states of matter that are either not known or are hard to achieve in thermal equilibrium. Classically, driven systems have been extensively studied in the framework of pattern formation and dynamics [1]. The study of quantum systems driven far from equilibrium is currently very active, in fields ranging from ultracold atoms [2–5] to optically induced superconductivity [6], and hybrid matter-light systems [7]. One such class of system is driven-dissipative lattices [8–10]. This is motivated by a variety of experimental platforms, including photonic crystal devices with quantum dots [11], micropillar structures in semiconductor microcavities [12], trapped ions [13], and microwave cavities and superconducting qubits [14,15]. Depending on the combination of couplings and driving used, many different models can be realized, and for many of these models, driving and dissipation allow one to induce a wider variety of collective states than occur in thermal equilibrium [16–25].

Most theoretical work on driven-dissipative lattices has focused on using order parameters or equal-time correlation functions to identify the phase diagram. For coherent driving, such observables correspond to measuring the elastically scattered light. Less attention has been paid to the properties of the incoherent fluorescence from such lattices. From the quantum optics perspective, incoherent fluorescence of a coherently driven system can reveal interactions and coherence times, as known for the Mollow triplet fluorescence [26], which has been seen in candidate systems for coupled cavity arrays such as quantum dots [27] and superconducting qubits coupled to microwave cavities [28]. In extended systems, one can also access momentum-resolved spectra, e.g., by measuring the interference of light emitted from different cavities. Moreover, second-order correlations distinguish bunching or antibunching of photons—as studied theoretically for a pair of coupled cavities [29,30]. Applied to extended systems, such measurements can make contact with quantities typically seen with condensed matter probes such as angle resolved photon emission, spectroscopic scanning tunneling microscopy, or neutron scattering; i.e., they measure the excitation and fluctuation spectrum of a correlated state, revealing the nature of correlated states.

There are other reasons to anticipate that calculations of two-point and two-time correlations can provide understanding beyond single-time observables. First, for any correct treatment of a finite size system, symmetry breaking should not occur. This can also be true for certain numerical approaches in infinite systems: unless one uses the noncommuting limits of symmetry-breaking fields and system size, one finds a steady state density matrix with equal mixtures of symmetry-broken states [31,32]. Two-time correlations allow one to instead ask how long symmetry breaking persists in response to a probe—i.e., long time correlations correspond to divergences of the zero frequency response of a system. For driven systems, similar results may be extended to the treatment of limit cycles and "nonequilibrium time crystals" [24,33,34]. The density matrix, as an ensemble averaged quantity, involves averaging over the phase (or equivalently origin in time) of any limit cycle, washing out any time dependence in the density matrix. In contrast two-time correlations reveal such cycles as a diverging response at nonzero frequency.

Another motivation for studying two-time correlations is to investigate thermalization. Thermalization in driven systems has been studied in a number of contexts, including the "low-energy effective temperature" in the Keldysh field theory of driven atom-photon systems [35–41] and the mode populations in photon [42,43] and polariton condensates [44–46]. This steady state behavior in a continuously driven system can also be connected to the emergence of a prethermalized state following a sudden

quench in an isolated system [47–49]—in such a prethermalized state, there is a flow of energy between degrees of freedom at different scales. For a thermalized state, we expect the density matrix takes the Gibbs form $\rho = \exp(-H_{\rm eff}/T_{\rm eff})$ with some effective Hamiltonian $H_{\rm eff}$. One may note, however, that *any* density matrix can be written in the Gibbs form; to make the criterion meaningful one thus needs a method to independently determine $H_{\rm eff}$. This means simultaneously measuring the occupations and densities of available states—this is the essence of the fluctuation-dissipation theorem, which we discuss below.

In this Letter, we find the two-time correlations of a driven-dissipative lattice, and see the emergence of a quasithermalized state. We calculate both on-site and intersite correlations, giving access to the momentum-resolved fluorescence spectrum of a driven coupled cavity array. In order to eliminate boundary and finite-size effects, we work always with the translationally invariant infinite lattice. On-site calculations in a finite-size lattice have also been recently studied for the XXZ model [50]. While the methods we present are general, our work will focus on the transverse-field anisotropic XY model (which has both the Ising and XY models as special cases), a driven-dissipative realization of which was proposed by Bardyn and İmamoğlu [51], and the steady state properties studied [20,52] using matrix product state approaches. As shown in [51] and reviewed in the Supplemental Material [53], this model can be realized by an array of coupled cavities in the photon blockade regime, with a two-photon pump that creates pairs of photons in adjacent sites (see Fig. 1).

Following [20,53], working in the rotating frame of the pump, the effective Hamiltonian has the form $H = -J\sum_j [g\sigma_j^z + [(1+\Delta)/2]\sigma_j^x\sigma_{j+1}^x + [(1-\Delta)/2]\sigma_j^y\sigma_{j+1}^y]$. The dimensionless transverse-field g depends on the pump-cavity detuning, and the anisotropy parameter Δ, given by the ratio of pump strength and photon hopping J. For $\Delta = 1$ we recover the Ising model and for $\Delta = 0$ the isotropic XY model. In the following, we will work in units of J. For the driven system, the Hamiltonian is accompanied by photon loss at rate κ into empty radiation modes. We thus have the master equation

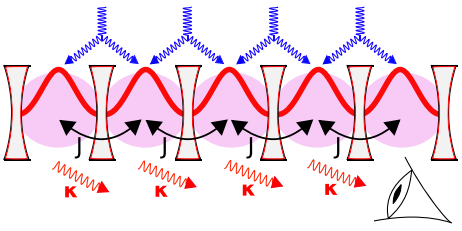

FIG. 1. Coupled cavity array with hopping J, photon loss κ, and two-photon pumping (blue line). When strong nonlinearity (purple shading) in each cavity leads to photon blockade, this yields the transverse-field anisotropic XY model [51].

$$\partial_t\rho = \mathcal{L}\{\rho\} = -i[H,\rho] + \frac{\kappa}{2}\sum_j (2\sigma_j^-\rho\sigma_j^+ - \sigma_j^+\sigma_j^-\rho - \rho\sigma_j^+\sigma_j^-). \quad (1)$$

While a nondriven system would equilibrate with the bath, the time-dependent driving breaks detailed balance and leads instead to a nonequilibrium steady state (NESS).

The fluctuation and response spectra discussed above require evaluating two-time correlation functions which, for a Markovian system, can be found using the quantum regression theorem [26]:

$$\langle O_2^{(j)}(t)O_1^{(i)}(0)\rangle = \mathrm{Tr}[O_2^{(j)}e^{t\mathcal{L}}O_1^{(i)}\rho_{\rm ss}], \quad (2)$$

where i, j label two lattice sites and 1,2 two local operators. In order to compute this for an infinite lattice, we employ matrix product state (MPS) methods. We first find the steady state $\rho_{\rm ss}$ of the master equation (1). We do this by using the infinite time evolving block decimation (ITEBD) algorithm [59,60] to find the translationally invariant infinite MPS such that $\mathcal{L}\{\rho_{\rm ss}\} = 0$. Starting from the NESS, we then calculate two-time correlations using Eq. (2). Because applying local operators $\hat{O}_1$ to $\rho_{\rm ss}$ breaks translational invariance, we can no longer propagate using ITEBD. For a finite size lattice, TEBD could be used, but this restricts the extent of correlations in both space and time, as excitations are reflected from the boundaries [61]. Fortunately, a method to find such correlations in an infinite lattice has been developed by Bañuls *et al.* [62] for unitary evolution. This approach [62], which we extend to open systems, writes the time evolution between applying $\hat{O}_1$ and $\hat{O}_2$ as a tensor network, and contracting this network gives the desired correlator (see [53] for details).

Using this approach, we calculate the fluctuation spectrum $S_{O,O^\dagger}(\omega)$ and the response function of the system $\chi''_{O,O^\dagger}(\omega)$ which are at the heart of the fluctuation-dissipation theorem [26,41], $S_{O,O^\dagger}(\omega) = F(\omega)\chi''_{O,O^\dagger}(\omega)$, with the distribution function $F(\omega)$ discussed below. Both $S_{O,O^\dagger}(\omega)$ and $\chi''_{O,O^\dagger}(\omega)$ are the Fourier transforms of two-time correlations

$$\tilde{S}_{O,O^\dagger}(t) = \frac{1}{2}\langle\{\hat{O}(t),\hat{O}^\dagger(0)\}\rangle, \quad (3)$$

$$\tilde{\chi}_{O,O^\dagger}(t) = i\theta(t)\langle[\hat{O}(t),\hat{O}^\dagger(0)]\rangle, \quad (4)$$

which we may evaluate using Eq. (2).

Figure 2 shows the on-site ($i = j$) fluctuation and response functions in frequency domain for $\hat{O}_1 = \hat{O}_2 = \hat{O} \in \{\sigma^x, \sigma^z\}$ and a range of values of transverse-field g. We show both the Ising limit ($\Delta = 1$, left two columns), as well as at small Δ (right column), where analytic results can be found using spin-wave theory as discussed further

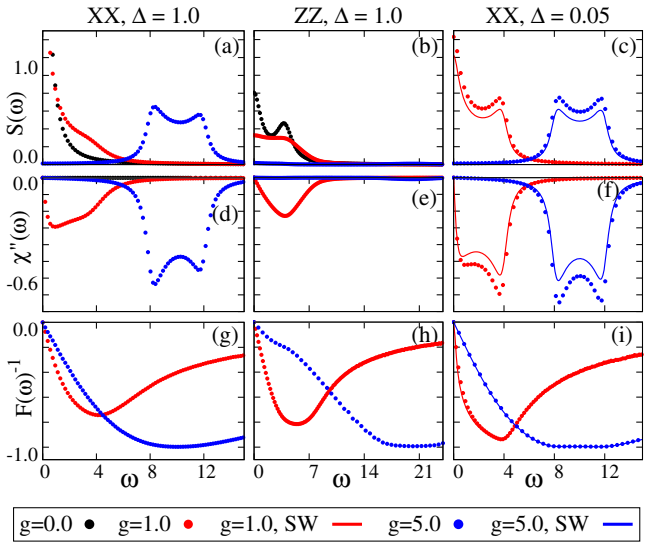

FIG. 2. Spectrum of fluctuations $S(\omega)$, imaginary part of response function $\chi''(\omega)$, and inverse distribution function $F(\omega)^{-1}$. Left two columns: Ising limit $\Delta = 1$. The right column shows $\Delta = 0.05$ where spin-wave theory (solid lines) matches well. Energies given in units of J. Other parameters used: $\kappa = 0.5$.

below. Panels (a)–(c) show $S(\omega)$ which measures the occupations, while panels (d)–(f) show response function $\chi''(\omega)$, which measures the density of states. We note that while at $g = 0$, 1 we see $S(\omega)$ for σ^x is peaked at $\omega = 0$, its value always remains finite as there is no phase transition in this open one-dimensional system [20,25]. As we will discuss later, the form of the density of states seen here can be understood from the momentum-resolved correlation functions.

The bottom row of Fig. 2 shows the inverse distribution functions $F(\omega)^{-1} = \chi''_{O,O^\dagger}(\omega)/S_{O,O^\dagger}(\omega)$ for $\hat{O} = \sigma^x, \sigma^z$, respectively. In an equilibrium system, the distribution function $F(\omega)$ depends only on whether $\hat{O}$ obeys fermionic or bosonic (anti-)commutation relations; for bosons it is: $F(\omega) \equiv 2n_B(\omega) + 1 = \coth[(\omega - \mu)/2T]$. In a driven-dissipative system, $F(\omega)$ may take a more general form. However, as identified in other contexts [7,35–41], quasi-thermalization of low-energy modes often occurs, leading to the identification of a low-energy effective temperature $F(\omega) \sim 2T_{\text{eff}}/\omega$. Note that since all calculations are performed in the rotating frame, all frequencies are measured relative to the pump frequency—i.e., the pump frequency acts as an effective chemical potential μ that sets the frequency at which $F(\omega)$ diverges.

As seen in Figs. 2(g) and 2(h), $F(\omega)^{-1}$ is linear $\omega \to 0$ indicating the emergence of a low-energy effective temperature in this model. Because the power spectrum of physical operators is positive, there is a minimum possible fluctuation contribution for a given dissipation, meaning $|F(\omega)|^{-1} \leq 1$. At high frequencies the distribution function of a fully thermalized system asymptotically approaches this value. In our nonequilibrium system we see that in some cases the inverse distribution $|F(\omega)|^{-1}$ approaches 1 over a range of frequencies; however, in all cases it falls below one at higher frequencies, indicating higher fluctuations than for a thermal state. The results shown give some indication that, at least for Fig. 2(g), the $F(\omega)$ approaches a thermal form more closely at larger g.

The right column of Fig. 2 compares the MPS results (points) to analytic spin-wave theory [53,63], which is valid if the density of excitations is small. We see a good agreement between spin-wave theory and MPS numerics at $\Delta = 0.05$ for σ^x correlations (we do not show the σ^z spectra for this Δ, as these vanish in the linearized spin-wave theory). Remarkably, the agreement for $F(\omega)$ is better than for $S(\omega)$, $\chi''(\omega)$ individually. It is notable that despite being a linear (i.e., noninteracting) theory, the spin-wave result reproduces both the low-energy effective temperature and the emergent plateau $F(\omega) \simeq 1$ at intermediate frequencies. The distribution function of spin-wave theory can be understood as a weighted average of k-dependent function $F(\omega, k) = (2T_{\text{eff},k} + \lambda_k\omega^2)/\omega$, with weighting by the k-dependent density of states [53]. This form (which follows directly from the structure of the relevant linearized theory) leads directly to the existence of a low-energy effective temperature. The plateau at $F(\omega) \simeq 1$, seen only at larger g, results from the local spectra averaging over many momentum states [53]; however, the form $F(\omega, k)$ inevitably leads to $F(\omega) \propto \omega$ at high frequencies, corresponding to the breakdown of the plateau.

As well as the deviation from the thermal $F(\omega)$, a second distinction from an equilibrated system is that both the distribution and the low-energy effective temperature extracted differ depending on the system operator considered. Figure 3(a) shows how T_{eff} of σ^x and σ^z correlators vary with transverse-field g. Figure 3(b) shows similar results for the spin-wave theory at small Δ for σ^x and σ^y correlators (as noted above, σ^z correlators vanish in a linearized theory). We observe that for $\Delta \to 0$, $g \to \infty$ the $\sigma^{x,y}$ excitations thermalize to the same effective

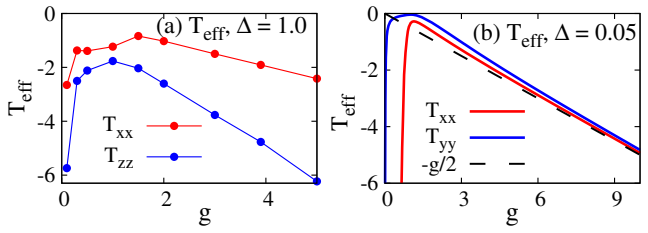

FIG. 3. The effective temperature T_{eff} against transverse-field g. We find T_{eff} by fitting $F(\omega) \simeq A\coth(b\omega)$ for low frequencies ($\omega \leq 1.0$), and plotting $T_{\text{eff}} \equiv A/2b$. (a) MPS results for $\sigma^{x,z}$ fluctuations and the transverse-field Ising limit ($\Delta = 1.0$); (b) spin-wave results for $\sigma^{x,y}$ fluctuations at $\Delta = 0.05$. Energies given in units of J. Other parameters used: $\kappa = 0.5$.

temperature, $T_{\text{eff}} \approx -g/2$. This can be understood as $T_{\text{eff},k}$ becomes k independent in this limit, see [53].

We only show results for $g > 0$ in Fig. 2, since there exists a simple duality allowing us to relate the form of $S(\omega)$, $\chi''(\omega)$, $F(\omega)^{-1}$ for values g and $-g$. This duality, discussed in [20] arises because a combination of $g \mapsto -g$ and a π rotation of the spin on every second site leads to $H \mapsto -H$. (A more general discussion of such dualities can be found in [64].) This duality means that on changing the sign of g, the state of the system should correspond to reversing the sign of all energies. We may then note that fluctuation and dissipation spectra show different parity; $\chi''(-\omega) = -\chi''(\omega)$, while $S(-\omega) = S(\omega)$, and so $F(-\omega) = -F(\omega)$. As such, the energy sign reversal under $g \mapsto -g$ yields a sign change of the distribution function and effective temperature. We find $g < 0$ gives positive temperatures, and $g > 0$ negative temperatures. This is consistent with the spatial ordering seen [20]: for $T_{\text{eff}} < 0$ there is a high energy antiferromagnetic state. A more intuitive understanding of this comes from the fact that g is proportional to the pump-cavity detuning, so that $g < 0$ corresponds to a red-detuned pump and consequent cooling, while $g > 0$ corresponds to blue detuning. Blue-detuned pumping is typically associated to heating; here it does lead to energy accumulation, but this induces a negative temperature state, rather than high positive temperatures. At $g = 0$, the susceptibility $\chi''(\omega)$ vanishes, so $F(\omega)^{-1} = 0$ and the effective temperature diverges.

So far, we have evaluated correlation functions at equal positions; this corresponds to recording all light from one cavity, which implicitly integrates over momentum. More information on the structure of the correlations is available if we consider the momentum-resolved spectrum. This requires evaluating correlations at nonequal sites i, j, and performing a double Fourier transform with respect to separation in time t and space $|i - j|$. The resulting fluctuation spectra $S(\omega, k)$ are displayed in Fig. 4 [the response function $\chi''(\omega, k)$ shows similar features as $S(\omega, k)$]. We show the case for $\hat{O} = \sigma^x, \sigma^z$, and two values of g (we consider only $g > 0$, since the duality discussed above allows one to understand the effects of a sign change of g). All the features visible in these spectra can be described straightforwardly using excitation spectra derived from the Jordan-Wigner solution of H_{TFI} (see, e.g., [65] for details).

At large positive g, the NESS is known [20] to be a maximum energy state with spins pointing in the $-\hat{z}$ direction, opposing the magnetic field. The spectrum of the σ^x operator corresponds to single spin flips, so it follows the single particle dispersion $\omega(k) = \epsilon(k) \equiv 2J\sqrt{1 + g^2 + 2g\cos(k)}$ (where we consider *deexcitations* of the *maximum* energy state). This expression is shown by the black line in Fig. 4(a). In contrast, the σ^z operator corresponds to two-particle excitations, which come in two varieties. The first one is a two-particle continuum with

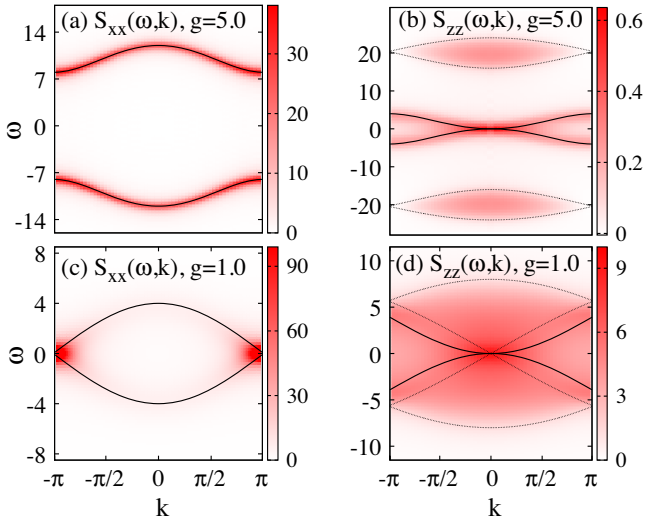

FIG. 4. $S(\omega, k)$ momentum-resolved fluctuation spectrum for excitations of (a) σ^x at $g = 5.0$; (b) σ^z at $g = 5.0$; (c) σ^x at $g = 1.0$; (d) σ^z at $g = 1.0$. Energies given in units of J. Other parameters used, $\kappa = 0.5$.

$\omega = \epsilon(k_1) + \epsilon(k_2), k_1 + k_2 = k$. The envelope of these states is given by $\epsilon_{\min}(k) < \omega(k) < \epsilon_{\max}(k)$ with $\epsilon_{\max/\min}(k) = 4J\sqrt{1 + g^2 \pm 2g\cos(k/2)}$, shown by the dotted black lines in Fig. 4(b). The other kind of excitations involves scattering existing particles from mode q to $q + k$, i.e., $\omega(k) = \Delta\epsilon(q, k) \equiv \epsilon(q + k) - \epsilon(q)$. The dominant contribution comes from $q = 0$, since this corresponds to the maximum energy mode, which is maximally occupied for a negative temperature state. The black solid line shows $\Delta\epsilon(0, k)$ which indeed matches the dominant feature observed. Given these momentum-resolved results, the momentum integrated spectral functions in Figs. 2(a) and 2(d) can be easily understood, with peaks arising from van Hove singularities at the band edges.

Near $g = 1.0$ the NESS instead shows antiferromagnetic correlations. The spectra here retain key features but are distorted. In the σ^x spectrum, Fig. 4(c) and Figs. 2(a) and 2(d), the peaks at $k = \pm\pi$ become dominant. In the σ^z spectrum, Fig. 4(d) and Figs. 2(b) and 2(e), the scattering band and two-particle continuum overlap. The black lines show the same expressions as discussed above. A ground state phase transition occurs for $|g| < 1$, hence the gap closing at $g = 1.0$. In contrast, the NESS at $g = 1.0$ already enters an antiferromagnetic state. As such, it is unsurprising these dispersions (which use normal state Jordan Wigner forms) do not match the spectrum as well as they did at $g = 1.0$. As one continues to decrease $g \to 0$ the spectrum becomes further dominated by the modes near $\omega = 0$, as seen in Figs. 2(a)–2(f).

In conclusion, we have calculated the two-time correlations of a driven-dissipative coupled cavity array, providing the fluorescence and absorption spectra. Because of the duality between red- and blue-detuned scenarios, we find

that a blue pump-cavity detuning produces a quasithermalized state with a negative temperature. We have also shown how the structure of $F(\omega)$ and emergent thermalization can be understood using a spin-wave theory, and how momentum-resolved fluorescence reveals the nature of quasiparticle excitations in the quasithermal state. The system we have studied here is in the photon blockade regime, with at most one excitation per site. This restricts us to study "first-order" correlation functions. When generalizing to problems with a larger on-site Hilbert space, second-order photon counting correlations may also be of interest, in revealing the coherence and statistics of any ordered state. Our results illustrate how calculating such correlations of the fluorescence can provide new insights into the state of many-body driven-dissipative systems.

The research data supporting this publication can be accessed at [66].

D. K. acknowledges support from the EPSRC CM-CDT (EP/L015110/1). J. K. acknowledges support from EPSRC program TOPNES (EP/I031014/1). We are grateful to M. Hartmann and S. H. Simon for helpful discussions, and to M. Hartmann for helpful comments on the manuscript.

[1] M. C. Cross and P. C. Hohenberg, Rev. Mod. Phys. **65**, 851 (1993).
[2] I. Bloch, J. Dalibard, and W. Zwerger, Rev. Mod. Phys. **80**, 885 (2008).
[3] H. Ritsch, P. Domokos, F. Brennecke, and T. Esslinger, Rev. Mod. Phys. **85**, 553 (2013).
[4] A. J. Daley, Adv. Phys. **63**, 77 (2014).
[5] T. Langen, R. Geiger, and J. Schmiedmayer, Annu. Rev. Condens. Matter Phys. **6**, 201 (2015).
[6] M. Mitrano, A. Cantaluppi, D. Nicoletti, S. Kaiser, A. Perucchi, S. Lupi, P. D. Pietro, D. Pontiroli, M. Ricc, S. R. Clark, D. Jaksch, and A. Cavalleri, Nature (London) **530**, 461 (2016).
[7] I. Carusotto and C. Ciuti, Rev. Mod. Phys. **85**, 299 (2013).
[8] S. Schmidt and J. Koch, Ann. Phys. (Berlin) **525**, 395 (2013).
[9] C. Noh and D. G. Angelakis, Rep. Prog. Phys. **80**, 016401 (2017).
[10] M. J. Hartmann, J. Opt. **18**, 104005 (2016).
[11] A. Majumdar, A. Rundquist, M. Bajcsy, and J. Vučković, Phys. Rev. B **86**, 045315 (2012).
[12] V. G. Sala, D. D. Solnyshkov, I. Carusotto, T. Jacqmin, A. Lemaître, H. Terças, A. Nalitov, M. Abbarchi, E. Galopin, I. Sagnes, J. Bloch, G. Malpuech, and A. Amo, Phys. Rev. X **5**, 011034 (2015).
[13] K. Toyoda, Y. Matsuno, A. Noguchi, S. Haze, and S. Urabe, Phys. Rev. Lett. **111**, 160501 (2013).
[14] A. A. Houck, H. E. Türeci, and J. Koch, Nat. Phys. **8**, 292 (2012).
[15] M. Fitzpatrick, N. M. Sundaresan, A. C. Y. Li, J. Koch, and A. A. Houck, Phys. Rev. X **7**, 011016 (2017).
[16] I. Carusotto, D. Gerace, H. E. Tureci, S. De Liberato, C. Ciuti, and A. İmamoğlu, Phys. Rev. Lett. **103**, 033601 (2009).
[17] M. J. Hartmann, Phys. Rev. Lett. **104**, 113601 (2010).
[18] T. Grujic, S. Clark, D. Jaksch, and D. Angelakis, New J. Phys. **14**, 103025 (2012).
[19] F. Nissen, S. Schmidt, M. Biondi, G. Blatter, H. E. Türeci, and J. Keeling, Phys. Rev. Lett. **108**, 233603 (2012).
[20] C. Joshi, F. Nissen, and J. Keeling, Phys. Rev. A **88**, 063835 (2013).
[21] J. Jin, D. Rossini, R. Fazio, M. Leib, and M. J. Hartmann, Phys. Rev. Lett. **110**, 163605 (2013).
[22] J. Jin, D. Rossini, M. Leib, M. J. Hartmann, and R. Fazio, Phys. Rev. A **90**, 023827 (2014).
[23] A. Biella, L. Mazza, I. Carusotto, D. Rossini, and R. Fazio, Phys. Rev. A **91**, 053815 (2015).
[24] M. Schiró, C. Joshi, M. Bordyuh, R. Fazio, J. Keeling, and H. E. Türeci, Phys. Rev. Lett. **116**, 143603 (2016).
[25] T. E. Lee, S. Gopalakrishnan, and M. D. Lukin, Phys. Rev. Lett. **110**, 257204 (2013).
[26] H.-P. Breuer and F. Petruccione, *The Theory of Open Quantum Systems* (Oxford University Press, Oxford, 2002).
[27] A. N. Vamivakas, Y. Zhao, C.-Y. Lu, and M. Atatüre, Nat. Phys. **5**, 198 (2009).
[28] C. Lang, D. Bozyigit, C. Eichler, L. Steffen, J. M. Fink, A. A. Abdumalikov, M. Baur, S. Filipp, M. P. da Silva, A. Blais, and A. Wallraff, Phys. Rev. Lett. **106**, 243601 (2011).
[29] T. C. H. Liew and V. Savona, Phys. Rev. Lett. **104**, 183601 (2010).
[30] M. Bamba, A. Imamoğlu, I. Carusotto, and C. Ciuti, Phys. Rev. A **83**, 021802 (2011).
[31] S. R. K. Rodriguez, W. Casteels, F. Storme, N. Carlon Zambon, I. Sagnes, L. Le Gratiet, E. Galopin, A. Lemaître, A. Amo, C. Ciuti, and J. Bloch, Phys. Rev. Lett. **118**, 247402 (2017).
[32] T. Fink, A. Schade, S. Höfling, C. Schneider, and A. İmamoğlu, Nat. Phys. **14**, 365 (2018).
[33] C.-K. Chan, T. E. Lee, and S. Gopalakrishnan, Phys. Rev. A **91**, 051601 (2015).
[34] F. Iemini, A. Russomanno, J. Keeling, M. Schirò, M. Dalmonte, and R. Fazio, Phys. Rev. Lett. **121**, 035301 (2018).
[35] S. Diehl, A. Micheli, A. Kantian, B. Kraus, H. Büchler, and P. Zoller, Nat. Phys. **4**, 878 (2008).
[36] S. Diehl, A. Tomadin, A. Micheli, R. Fazio, and P. Zoller, Phys. Rev. Lett. **105**, 015702 (2010).
[37] B. Öztop, M. Bordyuh, Ö. E. Müstecaplıoğlu, and H. E. Türeci, New J. Phys. **14**, 085011 (2012).
[38] E. G. D. Torre, S. Diehl, M. D. Lukin, S. Sachdev, and P. Strack, Phys. Rev. A **87**, 023831 (2013).
[39] M. Buchhold, P. Strack, S. Sachdev, and S. Diehl, Phys. Rev. A **87**, 063622 (2013).
[40] L. M. Sieberer, S. D. Huber, E. Altman, and S. Diehl, Phys. Rev. Lett. **110**, 195301 (2013).
[41] L. M. Sieberer, M. Buchhold, and S. Diehl, Rep. Prog. Phys. **79**, 096001 (2016).
[42] J. Klaers, J. Schmitt, F. Vewinger, and M. Weitz, Nature (London) **468**, 545 (2010).
[43] P. Kirton and J. Keeling, Phys. Rev. A **91**, 033826 (2015).
[44] T. D. Doan, H. T. Cao, D. B. Tran Thoai, and H. Haug, Phys. Rev. B **72**, 085301 (2005).

[45] J. Kasprzak, D. D. Solnyshkov, R. André, L. S. Dang, and G. Malpuech, Phys. Rev. Lett. **101**, 146404 (2008).
[46] Y. Sun, P. Wen, Y. Yoon, G. Liu, M. Steger, L. N. Pfeiffer, K. West, D. W. Snoke, and K. A. Nelson, Phys. Rev. Lett. **118**, 016602 (2017).
[47] A. Polkovnikov, K. Sengupta, A. Silva, and M. Vengalattore, Rev. Mod. Phys. **83**, 863 (2011).
[48] J. Eisert, M. Friesdorf, and C. Gogolin, Nat. Phys. **11**, 124 (2015).
[49] T. Langen, T. Gasenzer, and J. Schmiedmayer, J. Stat. Mech. (2016) 064009.
[50] S. Wolff, J.-S. Bernier, D. Poletti, A. Sheikhan, and C. Kollath, arXiv:1809.10464.
[51] C.-E. Bardyn and A. İmamoğlu, Phys. Rev. Lett. **109**, 253606 (2012).
[52] E. Mascarenhas, H. Flayac, and V. Savona, Phys. Rev. A **92**, 022116 (2015).
[53] See Supplemental Material at http://link.aps.org/supplemental/10.1103/PhysRevLett.122.043602 containing derivation of the effective model, details of the spin-wave calculation, and a full description of the tensor network method for two-time correlations, and also includes Refs. [54–58].
[54] M. O. Scully and M. S. Zubairy, *Quantum Optics* (Cambridge University Press, Cambridge, England, 1997).
[55] A. Altland and B. D. Simons, *Condensed Matter Field Theory* (Cambridge University Press, Cambridge, England, 2010).
[56] G. W. Ford and R. F. O'Connell, Phys. Rev. Lett. **77**, 798 (1996).
[57] E. Stoudenmire and S. R. White, New J. Phys. **12**, 055026 (2010).
[58] M. F. Maghrebi and A. V. Gorshkov, Phys. Rev. B **93**, 014307 (2016).
[59] U. Schollwöck, Ann. Phys. (Amsterdam) **326**, 96 (2011).
[60] R. Orús, Ann. Phys. (Amsterdam) **349**, 117 (2014).
[61] H. N. Phien, G. Vidal, and I. P. McCulloch, Phys. Rev. B **86**, 245107 (2012).
[62] M. C. Bañuls, M. B. Hastings, F. Verstraete, and J. I. Cirac, Phys. Rev. Lett. **102**, 240603 (2009).
[63] D. C. Mattis, *The Theory of Magnetism Made Simple: An Introduction to Physical Concepts and to Some Useful Mathematical Methods* (World Scientific Publishing Company, Singapore, 2006).
[64] A. C. Y. Li and J. Koch, New J. Phys. **19**, 115010 (2017).
[65] S. Sachdev, *Quantum Phase Transitions* (Cambridge University Press, Cambridge, England, 2007).
[66] https://doi.org/10.17630/e9294732-3515-411b-9e9f-05b777b86b2c.